IEEE Access
Multidisciplinary | Rapid Review | Open Access Journal

Received August 8, 2019, accepted August 23, 2019, date of publication September 24, 2019, date of current version October 22, 2019.

Digital Object Identifier 10.1109/ACCESS.2019.2943483

Global Robust Control Model of Friction Stir Welding of Aluminum Alloy Based on Main Motor Power Output Prediction

KUN ZHANG AND ZHENGJUN LIU
School of Materials Science and Engineering, Shenyang University of Technology, Shenyang 110870, China
Corresponding author: Kun Zhang (tlssys02@sut.edu.cn)

This work was supported by the Key Research Projects of Liaoning Province Higher Education under Grant LZGD2017037.

ABSTRACT Aiming at the softening problem of 7075 superhard aluminium welded joints such as hot cracks and gas holes in traditional fusion welding process, a dynamic robust control model based on the relationship between friction stir welding process parameters and welded joint strength is established. According to the non-linear relationship between global motion estimation and welded strength parameters, a dynamic robust control model of stirring needle motion is established, and the physical parameters such as elongation after fracture, tensile strength and hardness are calculated. A robust dynamic evolutionary optimization model of welding process parameters is established in the future to realize real-time optimization control of process parameters. On the basis of global motion control, the electric power output of the friction stir welding main motor is predicted according to the required line energy input of the stirring needle motion characteristics, and the real-time optimal control method of the motor electric power based on the expected thermal energy input of the welding process is established. A series of strength tests of welded joints based on the model show that the predicted results of the model can meet the needs of engineering and have practical value in engineering.

INDEX TERMS 7075 superhard aluminum alloy, friction stir welding, strength of welded joint, global dynamic robust control.

I. INTRODUCTION

7075 series aluminum alloy is widely used in aerospace, military, vehicle and other fields due to its high strength. The traditional riveting process has the advantages of easy operation and high tensile strength in high-strength aluminum alloy welding [1]–[3]. However, it is difficult to achieve the current lightweight requirements of the aluminum alloy structure due to the additional structural weight of the riveted joints. By using friction stir welding as solid phase welding, the problem of joint softening such as pores and hot cracks in the welding process caused by TIG or laser welding process can be well solved [4]–[6]. Scholars' optimization research on the performance of friction stir welded joints only focuses on the adjustment of welding process parameters or heat treatment methods, and the experimental simulations related to welding are not deep enough [7].

The associate editor coordinating the review of this manuscript and approving it for publication was Hao Luo.

Since friction stir welding involves metal plastic flow and deformation energy release process, the size of dynamic recrystallized grain decreases with increasing strain rate [8]. However, the relationship between the parameters of the dynamic recrystallization process and time must be nonlinear, and the motion of the friction stirrer corresponding to this should also be nonlinear.

During the friction stir welding process, the stirring needle is continuously moved in three dimensions, and the specimen itself also has slight displacement and vibration. Therefore, in the actual welding process, the mixing needle, the test piece, the plastic flowing metal in the weld and the metal during the deformation energy release process have their own movements, and the complex form of motion is mainly caused by the movement of the agitating needle. This paper refers to it as frictional friction global motion.

Aiming at the metal plastic flow and its thermodynamic nonlinear characteristics during high-hardness aluminum alloy welding process are studied. The global motion robust control model of friction stir welding which can fit the plastic

flow of the weld metal and the nonlinear process of cooling is studied, and the dynamic optimization control of the welding process is implemented. The tensile strength of the welded joint after welding is compared with the tensile strength of the friction stir welded joint with the traditional fixed parameters to improve the welding quality.

In this paper, 7075 super-hard aluminum is used as the experimental plate. Under the condition that the rotation direction and angle of the mixing head are kept constant at 2.5°, the motion law of metal plastic flow and deformation energy release during friction stir welding is found by global motion control. First, global motion estimation is performed to obtain the vibration and displacement parameters of the test piece. Then, according to the temperature of the test piece, the plasticizing flow of the weld metal and the change of the grain size of the dynamic recrystallization, the stirring needle is motion compensated. The next moment movement parameter of the stirring needle can be obtained, and the ideal movement state of the stirring needle can be realized. Aiming at the line energy input control problem in the welding process, the main motor power robust estimation model is established to determine the optimal motor energy output power prediction value to ensure that the required input thermal power meets the global motion control requirements during the online energy control period. The strength test of welded joints shows that the prediction results of the model can meet the engineering needs and have practical value.

II. ROBUST ESTIMATION MODEL FOR FRICTION STIR WELDING GLOBAL MOTION STATE

According to the principle of friction stir welding, the agitating needle is rotated at a certain speed during the welding process to be inserted into the joint interface of the material to be welded, and subjected to a certain downward pressure. And the frictional heat between the rotating stirring head and the test piece causes strong plastic deformation of the material in the advancing direction of the stirring head [9], [10].

The shoulder can not only rub against the surface of the welding material to generate frictional heat, but also prevent the mixing head from spraying the plasticized base material from the weld zone at high speed, and at the same time, it can remove the oxide film on the surface of the material to be welded. As the mixing head moves, the highly plastically deformed material flows to the back of the mixing head, and the material behind the mixing head cools to form a solid weld [11]–[13].

According to the TIG welding control principle shown in Figure 1, the nozzle and the wire are advanced at a certain speed during the welding process and inserted into the arc at the interface where the tungsten electrode is bonded to the material to be welded. This paper defines the agitator needle motion rectangular coordinate system as: take the center line of the weld as the horizontal axis (x axis), and take the straight line of the weld welding starting point parallel to the axis of the stirring needle as the vertical axis (y axis) to form a rectangular coordinate system. According to the definition

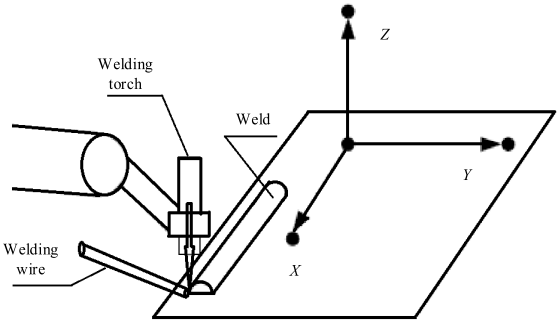

FIGURE 1. TIG welding control schematic.

of the stirring needle motion coordinate system, the x-axis is the direction of the agitation needle forward speed, the y-axis is the axial pressure direction, and the y-axis is also the agitating needle rotation axis. The position vector of the agitating needle in its motion coordinate system is defined as $v = (x, y)$

According to the principle of friction stir welding process, the mathematical model describing the state of friction stir motion is defined as:

$$F(v, t) \tag{1}$$

where: t is time; v is the position vector during the stirring needle movement. During the movement of the agitating needle, the relationship between the position vectors (x, y) and (x', y') of the agitating needle between the two moments can be expressed as:

$$\begin{cases} x' = ax + by + c \\ y' = dx + ey + f \end{cases} \tag{2}$$

Stirring needle global motion vector is defined as:

$$M = (a, b, c, d, e, f)T \tag{3}$$

where: c, f are the forward motion relationship parameter of the stirring needle at two adjacent moments.; a, b are the axial motion relationship parameter of the stirring needle at two adjacent moments; d, e are the rotational motion relationship parameter of the stirring needle at two adjacent moments.

According to the global motion vector M and the frictional friction motion state $F(v, t)$ at time t, the global motion state at time $t + \Delta t$ is: $F(v, t + \Delta t, M)$. The position of the stirring needle position in $F(v, t)$ and $F(v, t + \Delta t, M)$ satisfies the following relationship:

$$\begin{cases} F[v(t + \Delta t), t + \Delta t, M] = F[v(t), t] \\ x(t) = ax\,(t + \Delta t) + by\,(t + \Delta t) + c \\ y(t) = dx\,(t + \Delta t) + ey\,(t + \Delta t) + f \end{cases} \tag{4}$$

where: $v(t + \Delta t) = [x(t + \Delta t),\ y(t + \Delta t)]T$, $v(t) = [x(t),\ y(t)]T$.

From equation (4), the global motion state estimation of the agitating needle is to solve the most global motion vector M, the $F(r, t + \Delta t, M)$ of the frictional motion state model under the global motion vector M of equation (1) is most similar to

optimal frictional friction state $F(r, t + \Delta t)$ in the welding process under the least squares criterion.

III. DYNAMIC ROBUST CONTROL MODEL FOR AGITATING NEEDLE MOTION

According to the principle of friction stir welding, under a certain axial pressure, the advance speed of the stirring head is generally 70-100 mm/min, the rotating speed is generally 800-1000 r/min, and the welding process is generally 10-30 min [14]. Therefore, in order to realize the dynamic control of the friction stir welding process and to satisfy the robustness of the control model within the range of mechanical, physical and chemical factors, it is necessary to make a real-time and accurate estimation of the motion state of the stirring needle during the welding process. The Gauss-Newton (GN) method or the LM method used for motion control have good convergence, but the calculation amount is large, so it is not conducive to the fast dynamic calculation of the stirring needle motion state during the welding process. Aiming at this problem, the dynamic motion robust control algorithm of the stirring needle based on Gauss-Newton method is proposed.

Assume that the position vector of the stirring needle in the motion coordinate system is $[X(t), Y(t)]T$ at time t. Then, the position vector of the stirring needle in the coordinate system is $[X(t + \Delta t), Y(t + \Delta t)]T$ at the next moment, and the position of the stirring needle at two moments satisfies the following relationship:

$$\begin{cases} X(t) = aX\left(t + \Delta t\right) + bY\left(t + \Delta t\right) + c \\ Y(t) = dX\left(t + \Delta t\right) + eY\left(t + \Delta t\right) + f \end{cases} \tag{5}$$

The dual relationship of the above formula is:

$$\begin{aligned} \begin{bmatrix} X\left(t + \Delta t\right) \\ Y\left(t + \Delta t\right) \end{bmatrix} &= \begin{bmatrix} a & b \\ d & e \end{bmatrix}^{-1} \left\{ \begin{bmatrix} X(t) \\ Y(t) \end{bmatrix} - \begin{bmatrix} c \\ f \end{bmatrix} \right\} \\ &= \begin{bmatrix} a' & b' \\ d' & e' \end{bmatrix} \begin{bmatrix} X(t) \\ Y(t) \end{bmatrix} + \begin{bmatrix} c' \\ f' \end{bmatrix} \end{aligned} \tag{6}$$

where:

$$\begin{bmatrix} a' & b' \\ d' & e' \end{bmatrix} = \begin{bmatrix} a & b \\ d & e \end{bmatrix}^{-1}$$

$$\begin{bmatrix} c' \\ f' \end{bmatrix} = -\begin{bmatrix} a & b \\ d & e \end{bmatrix}^{-1} \begin{bmatrix} c \\ f \end{bmatrix}$$

If Δt is small enough, it can be assumed that the temperature of all points in the metal multiphase thermodynamic system at two times is constant.

Under the condition of constant temperature, it is assumed that there are N possible positions of the stirring needle position vector in the rectangular coordinate system of the stirring needle motion at $t + \Delta t$, and the relationship between the N position vectors is:

$$\begin{cases} I\left(X_1(t), Y_1(t), t\right) = I\left(X_1\left(t + \Delta t\right), Y_1\left(t + \Delta t\right), t + \Delta t\right) \\ I\left(X_2(t), Y_2(t), t\right) = I\left(X_2\left(t + \Delta t\right), Y_2\left(t + \Delta t\right), t + \Delta t\right) \\ \quad \vdots \qquad\qquad\qquad\qquad \vdots \\ I\left(X_i(t), Y_i(t), t\right) = I\left(X_i\left(t + \Delta t\right), Y_i\left(t + \Delta t\right), t + \Delta t\right) \\ \vdots\!\vdots \\ I\left(X_N(t), Y_N(t), t\right) = I\left(X_N\left(t+\Delta t\right), Y_N\left(t+\Delta t\right), t+\Delta t\right) \end{cases} \tag{7}$$

where: i is the i-th vector point where the stirring needle is in the motion coordinate system. Equation (7) is a super-constrained equation system. The number of unknowns is 6, and the total number of equations is N. Then equation (7) can not find an exact solution. Set $\vec{F}$ denote the vector matrix formed by the position vector of the stirring needle at the time of (t + 1), and $\vec{F}(M)$ denote the operational state estimation matrix under the global motion vector M, then:

$$\begin{aligned} \vec{F} = [&F\left(X_0\left(t + \Delta t\right), Y_0\left(t + 1\right)\Delta t, t + \Delta t\right), \\ &\times F\left(X_0\left(t + \Delta t\right), Y_0\left(t + \Delta t\right), t + \Delta t\right), \ldots, \\ &\times F\left(X_{N-1}\left(t + \Delta t\right), Y_{N-1}\left(t + \Delta t\right), t + \Delta t\right)]^T \end{aligned} \tag{8}$$

$$\begin{aligned} \vec{F}\left(M\right) = [&F\left(X_0(t), Y_0(t), t\right), \\ &\times F\left(X_0(t), Y_0(t), t\right), \ldots, \\ &\times F\left(X_{N-1}(t), Y_{N-1}(t), t\right)]^T \end{aligned} \tag{9}$$

The calculated value $I\left(X_i(t), Y_i(t), t\right)$ of the optimal position vector of the stirring needle is expanded at the true value $I\left(X_i\left(t + \Delta t\right), Y_i\left(t + \Delta t\right), t + \Delta t\right)$ at the time $t + \Delta t$:

$$\begin{aligned} \left(X(t), Y(t), t\right) = &F\left(X\left(t + \Delta t\right), Y\left(t + \Delta t\right), t + \Delta t\right) \\ &+ \frac{\partial F}{\partial X\left(t+\Delta t\right)} \left(X'\left(t+\Delta t\right) - X\left(t+\Delta t\right)\right) \\ &+ \frac{\partial F}{\partial Y\left(t+\Delta t\right)} \left(Y'\left(t+\Delta t\right) - Y\left(t+\Delta t\right)\right) \end{aligned} \tag{10}$$

where: $(X'(t + \Delta t), Y'(t + \Delta t))$ is the position vector of the stirring needle position vector at the time t at the stirring motion coordinate system of $(X(t), Y(t))$ at $t+\Delta t$. According to the formula (6), $(X'(t+\Delta t), Y'(t+\Delta t))$ in the formula (10) is represented by $(X(t + \Delta t), Y(t + \Delta t))$, then:

$$\begin{aligned} \Delta\vec{F} = &F_X X(t + \Delta t)(a' - 1) \\ &+ F_X Y(t + \Delta t)b' + F_X c' \\ &+ F_{_Y} X(t + \Delta t)d' \\ &+ F_Y Y(t + \Delta t)(e' - 1) + F_Y f' \end{aligned} \tag{11}$$

where: $F_X = \frac{\partial F}{\partial X(t+\Delta t)}$, $F_Y = \frac{\partial F}{\partial Y(t+\Delta t)}$,

$$\Delta F = F\left(X(t + \Delta t), Y(t + \Delta t), t + \Delta t\right) - F\left(X(t), Y(t), t\right)$$

Each feasible stirring needle position vector has an equation (11) as a constraint, and the constrained equations thus obtained are also super-constrained equations. However,

the parameters cannot be solved directly, and the matrix needs to be used to represent the equation:

$$\begin{aligned} M &= \left[a' - 1, b', c', d', e' - 1, f'\right]^{\mathrm{T}} \\ &= M' - [1, 0, 0, 0, 1, 0]^T \end{aligned} \tag{12}$$

Then there is:

$$P = \begin{bmatrix} F_{X1}X_1 & F_{X1}Y_1 & F_{Y1}Y_1 & F_{Y1} \\ \vdots & \vdots & \vdots & \vdots \\ F_{XN}X_N & F_{XN}Y_N & F_{YN}Y_1 & F_{YN} \end{bmatrix}$$

Available from formula (11):

$$PM' = \Delta F$$

The energy function of the deformation energy change during the welding process is defined as:

$$E = \left(\Delta F - PM'\right)^T W \left(\Delta F - PM'\right)$$

where: W is the weight matrix. M is a diagonal matrix, and its diagonal element W_i represents the weight of the i-th possible agitating needle position vector to the deformation energy of the weldment.

Set:

$$\frac{\partial E}{\partial M'} = 0$$

According to the above formula can be derived:

$$M' = \left(P^T WP\right)^{-1} \left(P^T W \left(\Delta F\right)\right) \tag{13}$$

According to formula (12):

$$M' = M + [1, 0, 0, 0, 1, 0]^{\mathrm{T}}$$

Set: $M_1 = (a_1, b_1, c_1, d_1, e_1, f_1)^T$, From equation (11), we can get:

$$\begin{bmatrix} a_1 & b_1 \\ d_1 & e_1 \end{bmatrix} = \begin{bmatrix} a' & b' \\ d' & e' \end{bmatrix}$$

$$\begin{bmatrix} c_1 \\ f_1 \end{bmatrix} = -\begin{bmatrix} a' & b' \\ d' & e' \end{bmatrix}^{-1} \begin{bmatrix} c' \\ f' \end{bmatrix}$$

Then, according to M_1 and M, the global motion vector model between the $t + \Delta t$ time and the t-time stirring needle position vector of the first iteration is:

$$\begin{aligned} \begin{bmatrix} X(t) \\ Y(t) \end{bmatrix} &= \begin{bmatrix} a & b \\ d & e \end{bmatrix} \left(\begin{bmatrix} a_1 b_1 \\ d_1 e_1 \end{bmatrix} \begin{bmatrix} X(t+1) \\ Y(t+1) \end{bmatrix} + \begin{bmatrix} c_1 \\ f_1 \end{bmatrix} \right) \\ &\quad + \begin{bmatrix} c \\ f \end{bmatrix} \\ &= \begin{bmatrix} a & b \\ d & e \end{bmatrix} \begin{bmatrix} a_1 & b_1 \\ d_1 & c_1 \end{bmatrix} \begin{bmatrix} X(t+1) \\ Y(t+1) \end{bmatrix} \\ &\quad + \begin{bmatrix} a & b \\ d & e \end{bmatrix} \begin{bmatrix} c_1 \\ f_1 \end{bmatrix} + \begin{bmatrix} c \\ f \end{bmatrix} \end{aligned} \tag{14}$$

From the above formula, the stir needle global motion control vector M^1 obtained in the first iteration can be obtained:

$$M^1 = \begin{bmatrix} a^1 \\ b^1 \\ c^1 \\ d^1 \\ e^1 \\ f^1 \end{bmatrix} = \begin{bmatrix} aa_1 + bd_1 \\ ab_1 + be_1 \\ ac_1 + bf_1 \\ da + ed_1 \\ db_1 + ee_1 \\ dc_1 + ef_1 + f \end{bmatrix}$$

Iteratively solve according to equation (12) until the end condition is met. Then, the optimal global motion vector M of the stirring needle at time t and time $t + 1$ is obtained.

According to the formula (4) in the previous section, the optimal position vector $F(v, t + \Delta t, M)$ at the next moment can be obtained. Since the position of the stirring needle is determined by three parameters: axial stress, rotational speed and forward speed. Then, after obtaining the optimal position vector, the parameters of the stirring needle can be controlled according to the optimal position vector.

IV. ROBUST ESTIMATION MODEL FOR MAIN MOTOR POWER OUTPUT

A. MAIN MOTOR POWER ROBUST ESTIMATION MODEL

The line energy of the energy input of the welding process is expressed as:

$$q_{EIN} = \frac{Q_{IN}}{v_{IN}} = k_{IN}\mu_{IN}F_{IN}\frac{n_{IN}}{v_{IN}} \tag{15}$$

where, P_{IN} is the motor output power, k_{IN} is the electric heating power conversion coefficient, μ_{IN} is the friction factor, n_{IN} is the stirring head speed, F_{IN} is the welding pressure; v_{IN} is the welding speed.

In a line energy control period, for the global motion vector M with uncertainty, the predicted power Q_{IN} and its probability c that the main motor of the friction stir welding equipment should output are calculated in real time. In the actual friction stir welding process, the main motor will output the actual power of size r. At the end of a line energy control period, for the case where the motor output power is less than the thermal power, the under-input of the welding process line energy will be Q_{INS}, If the motor output power is greater than its corresponding thermal power, the over-input amount of the welding line energy will be Q_{INV}.

The line energy input control problem in the welding process can be converted into an optimal motor energy output power predicted value Q^* at the beginning of the online energy control period to ensure that the required input thermal power meets the global motion control requirements during the online energy control period.

Under the premise that the stirring head motion control parameter is known and its corresponding thermal power input quantity and its probability distribution form are unknown, the motor output power control scene d is divided into m scenes according to the line energy control cycle time length:

$$d \in \{d_1, d_2, \ldots, d_m\} \tag{16}$$

The value of each scene $d_i\,(i = 1, 2, \ldots\ldots, m)$ corresponds to a line energy control time length. Set the probability of the motor output power predicted value and the thermal power error of $e_i\,(i = 1, 2 \ldots\ldots, m)$ in the d_i scene be $P_r(d = d_i) = p_i$, respectively. Where $p_i \geq 0$, $\sum_{i=1}^{m} p_i = 1$.

In order to make the main motor output power prediction value Q accurately reflect the actual heat input power under the welding process line energy control scenario d, the fitness function is defined as:

$$\zeta\,(Q; d) = r \min\,(d, Q) - P_s \cdot \max\,(d - Q) + \max\,(Q - d) - c \cdot Q \quad (17)$$

The optimal output power of the motor is:

$$Q^* = \arg\min \left\{ E\left[\zeta\,(Q; d)\right] = \sum_{i=1}^{m} p_i \zeta\,(Q; d_i) \right\} \quad (18)$$

where, $E[\cdot]$ is the expectation operator.

Set $p = (p_1, p_2, \ldots\ldots, p_m)^{\mathrm{T}}$ represent the unknown probability vector of the error between the motor output power prediction and the required thermal power at a future time. Then, under the uncertain probability distribution of the motor output power prediction error, the problem of robust estimation of motor output power can be expressed as:

$$\begin{aligned} &\max_{Q,\alpha_Q} \min_{\boldsymbol{p}} \left\{ \alpha_Q - \frac{1}{\beta} E\left\{ \max\left[\alpha_Q - \zeta\,(Q; d)\right] \right\} \right\} \\ &= \max_{Q,\alpha_Q} \min_{\boldsymbol{p}} \left\{ \alpha_Q - \frac{1}{\beta} \sum_{i=1}^{m} p_i \cdot \max\left[\alpha_Q - \zeta\,(Q; d)\right] \right\} \end{aligned} \quad (19)$$

where β is the fitness risk tolerance, expressed as the probability that the motor output power is less than the thermal power required for the welding process. α_Q is the threshold of the fitness function $\xi(Q; d)$.

Set auxiliary vector $u = (u_1, u_2, \ldots\ldots, u_{\mathrm{m}})^{\mathrm{T}}$, and equation (19) can be transformed into a robust optimization problem:

$$\begin{cases} \max\limits_{Q,\alpha_Q,\vartheta,u} \\ s.t.\ \min\limits_{p} \alpha_Q - \frac{1}{\beta} p^{\mathrm{T}} u \geq \vartheta \\ \quad u_i \geq \alpha_Q - \zeta\,(Q; d_i)\,, i = 1, 2, \ldots, m \\ \quad u_i \geq 0, i = 1, 2, \ldots, m \end{cases} \quad (20)$$

where, $(Q, \alpha_Q, \vartheta, u) \in R \times R \times R \times R^m$.

B. ROBUST ESTIMATION MODEL FOR MAIN MOTOR OUTPUT POWER

Since equation (20) contains an unknown probability vector p, it is difficult to solve directly. This paper is aimed at predicting the error probability of motor output power with uncertainty. Converting the above optimization problem into a confidence estimate of the motor output power prediction confidence domain that satisfies a certain confidence level, namely, the optimum issue of Equation (20) is turned into the issue robust plan.

Set the motor output power prediction error be the probability vector of the scene of each line energy control period length $p = (p_1, p_2, .., p_m)^{\mathrm{T}} \geq 0$. The probability vector of the motor output power prediction credibility in each scene corresponding to it is $q = (q_1, q_2, .., q_m)^{\mathrm{T}} \geq 0$. The divergence function between the motor output power prediction reliability and the motor output power prediction error probability is χ^2-distance function [15]:

$$I_\phi\,(p, q) = \sum_{i=1}^{m} q_i \phi\left(\frac{p_i}{q_i}\right) \quad (21)$$

The prediction results of the m motor output powers obtained by the friction stir welding process are: d_1, $d_2, \ldots, d_m$, and N samples of the prediction result scene are obtained. At the confidence level 1-K, the confidence domain of the motor output power prediction confidence probability p in each scenario is:

$$\mu_N = \left\{ p \in R^m \,\middle|\, p \geq 0, e^{\mathrm{T}} p = 1, I_\phi(p, \hat{p}_N) \leq p \right\} \quad (22)$$

where, $e^{\mathrm{T}} = (e_1, e_2, \ldots, e_m)$ is the error vector of the motor output power prediction in each scene. $\hat{p}_N = (p_{1,N}, p_{2,N}, \ldots, p_{m,N})$ is the maximum likelihood estimate of the probability p on the basis of N samples. For a small sample size N:

$$p = \frac{\phi''(1)}{2N}(\sqrt{\delta_\phi}\chi^2_{m-1,1-k} + \gamma_\phi)$$

where, δ_φ and γ_φ are correction parameters, and ϕ'', ϕ''' and ϕ'''' are second-order, third-order, and fourth-order derivatives.

$$\begin{aligned} \delta_\phi &= 1 + \frac{1}{2\,(m-1)\,N} \left\{ \left(2 - 2m - m^2 + s\right) \right. \\ &\quad + \frac{2\phi''\,(1)}{\phi''\,(1)} \left(4 - 6m - m^2 + 3s\right) \\ &\quad + \frac{1}{3} \left(\frac{\phi'''\,(1)}{\phi''\,(1)}\right)^2 \left(4 - 6m - m^2 + 5s\right) \\ &\quad \left. + \frac{2\phi''''\,(1)}{\phi''\,(1)} (1 - 2m + s) \right\} \\ \gamma_\phi &= (m-1) \left(1 - \sqrt{\delta_\phi}\right) \\ &\quad + \frac{1}{N} \left(\frac{\phi'''\,(1)}{3\phi''\,(1)} (2 - 3m + s) + \frac{\phi''''\,(1)}{4\phi''\,(1)} (1 - 2m + s) \right) \end{aligned}$$

where, s is used as an auxiliary parameter, and $s = \sum_{i=1}^{m} \frac{1}{p_{i,N}}$

Then under the uncertain probability set, the minimum constraint problem of equation (6) is transformed into:

$$\begin{cases} \alpha_Q - \eta - \lambda\rho - \lambda \sum_{i=1}^{m} p_{i,N} \phi^*\left(\frac{\beta^{-1}\mu_i - \eta}{\lambda}\right) \geq \vartheta \\ \lambda \geq 0 \end{cases} \quad (23)$$

TABLE 1. Chemical composition of base metal(Percentage by mass, %).

ingredient	Si	Cu	Mg	Mn	Zn	Al
standard value	≤0.4	1.2-2.0	2.1-2.9	≤0.30	5.1-6.1	margin
Measured value	0.07	1.56	2.54	0.031	5.77	margin

TABLE 2. Welding procedure parameter.

Serial number	rotation speed w/(r·min^{-1})	forward speed (v/(mm·min^{-1})	axial stress δ/Mp	Motor output power Q/kW
1	1000	50	156	3.2
2	1000	70	155	3.3
3	1000	100	158	4.6
4	1000	120	156	5.1
5	1000	140	156	6.6

where, ϕ^* is the conjugate function of function ϕ. Then the parameter optimization problem of equation (6) is transformed into a robust programming problem:

$$\begin{cases} \max\limits_{Q,\vartheta,\lambda,\eta,u} \ \vartheta \\ \text{s.t. } \alpha_Q - \eta - \lambda\rho - \lambda \sum\limits_{i=1}^{m} p_{i,N}\phi^*\left(\dfrac{\beta^{-1}\mu_i - \eta}{\lambda}\right) \geq \vartheta, \\ \quad u_i \geq \alpha_Q - \zeta(Q; d_i), i = 1, 2, \cdots, m, \\ \quad u_i \geq 0, i = 1, 2, \cdots, m, \\ \quad \lambda \geq 0 \end{cases} \tag{24}$$

where, $(Q, \vartheta, \lambda, \eta, u) \in R \times R \times R \times R \times R \times R^m$.

V. TEST AND RESULT ANALYSIS VERIFICATION

In order to obtain the flawless welded joints with the best tensile strength, it is preferred to use the optimum welding process parameters and the ratio of ω/v. The AA7075 test panels used in the paper are as shown in Table 1. Welding parameters are shown in Table 1.

For the tensile test, a non-standard sample of the size shown in Figure 2 was used. Two samples were taken for each specification parameter, and the SANS type electronic universal testing machine was used for the tensile test at room temperature. The gauge length was set to 30 mm and the tensile rate was 0.5 mm/min. The tensile strength was calculated from the average of the tensile deformation length of the two samples.

Five sets of friction stir welding without motion control and 5 sets of friction stir welding with motion control were carried out. After applying the global motion robust control, the comparison between the motion state of the stirring needle and the motion state of the stirring needle without the application of robust control is shown in Figure 3.

As shown in Figure 4, due to the application of the motion control, the traveling state of the agitating needle during the welding process is adjusted in real time according to

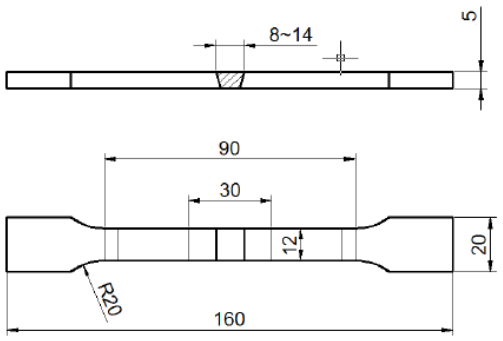

FIGURE 2. Dimension of non-standard tensile specimens(mm).

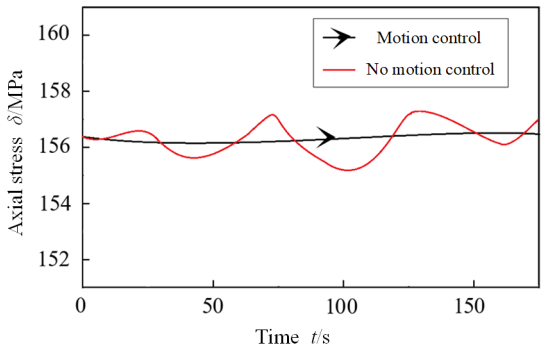

FIGURE 3. Comparison of motion control processes.

TABLE 3. Mechanical properties of welded joints.

Test group		Tensile strength R_m/MPa	Average hardness H(HV)
No motion control	1	368	116
	2	376	121
	3	397	126
	4	413	132
	5	424	128
Motion control	6	382	117
	7	385	122
	8	418	125
	9	422	131
	10	443	126

the welding process. In the welding process without the application of robust control, the parameters of the stirring needle are relatively small.

After the welding is finished, the tensile strength test is performed on the welded parts to compare the effects of the motion control. It can be seen from Table 3 that the global dynamic robust control of the stirring needle movement can effectively improve the tensile strength of the 7075 superhard aluminum alloy welded joint. The test results are shown in Figure 4 and Figure 5. The experimental results of the rotation speed and the forward speed are the group numbers.

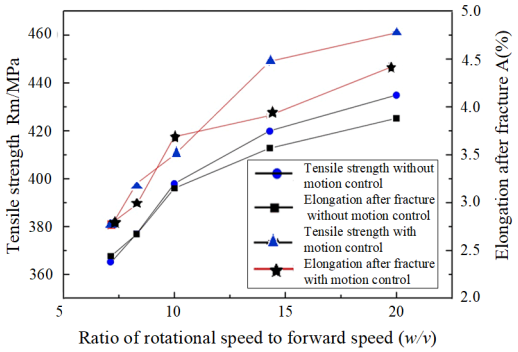

FIGURE 4. Tensile strength and elongation of welded joints before and after motion control.

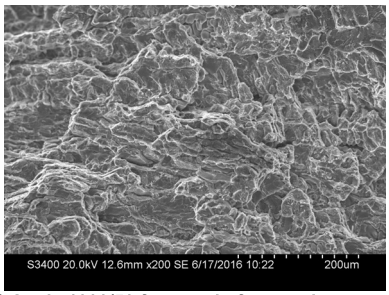

(a) Apply 1000/50 fracture before motion control

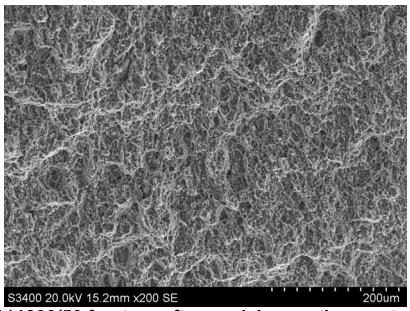

(b)1000/50 fracture after applying motion control

FIGURE 5. Welding joint fracture before and after motion control.

Figure 5a shows the fracture morphology of the welded joint obtained under the welding process parameters of the rotation speed of 1000r/min and the forward speed of 50mm/min, showing the fracture mode of the cleavage tongue type. This is because twins hinder the advancement of cracks. In the separation of twins and substrates, the cracks deviate from the original expansion direction. These dimples are evenly distributed, and the morphology is small and deep. The fracture is composed of dimples with large differences in size and size, showing the characteristics of pore accumulation. The small dimples are shallow and evenly distributed, and the large dimples contain broken particles. This is because during the stretching process, holes are formed inside the aluminum plate, and under the action of displacement, the holes become larger and are connected with other holes.

Figure 5b shows the fracture morphology after applying the motion control under the same welding process parameters, showing the traces of the deformation arc. The fracture

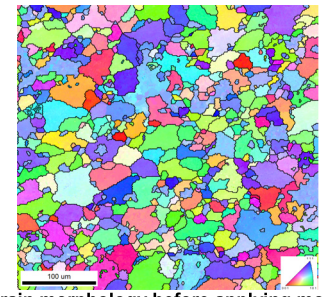

(a)EBSD grain morphology before applying motion control

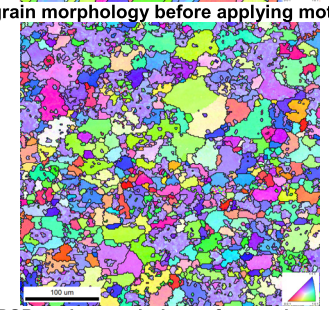

(b)EBSD grain morphology after motion control

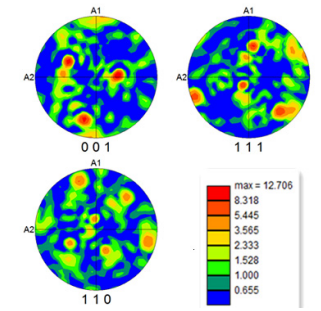

(c)Polar map before applying motion control

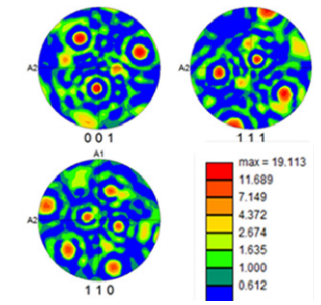

(d)Pole diagram after applying motion control

FIGURE 6. 1000/120 EBSD results of welding joint.

consists of a dimple with a large difference. The large dimple contains many broken particles, and the dimple is caused by the accumulation of pores.

Figure 6 is the EBSD organization diagram of the fracture morphology of the welded joint obtained under the welding process parameters of the rotation speed of 1000r/min and the forward speed of 120mm/min. 7075 aluminum alloy is used as a face-centered cubic structural material. During the friction stir welding process, the (111) surface is almost parallel to the cutting plane of the stirring needle, and parallel to the tangent of the stirring needle is the [110] direction. It can be seen from Figure 6a and Figure 6b that there are a small amount of twinned microstructures in both sets of

samples, and the grains are finer under the robust control conditions of the friction stir process. As can be seen from Figures 6c and 6d, the [110] silk texture was formed under the rotary extrusion of the stirring needle, and a (110) [001] Gaussian texture was also formed. Under the robust control condition of the friction stir process, the (110)[001] Gaussian orientation has more grain components, and the grain orientation of the grains is rotated by a certain angle along the <111> crystal orientation.

VI. CONCLUSION

(1) Friction stir welding can improve the quality of welded joints of 7075 to some extent, but in the welding parameters, the rotation speed and forward speed of the mixing head are not single constant, and the other can be adjusted moderately. The ratio of the two changes within a certain range, showing a nonlinear jump.

(2) The global robust optimization model of the friction stir welding process parameters is established, and the speed stress of the stirring needle is monitored and optimized in real time during the process of friction stir processing, which can effectively control the grain crystallization characteristics of the weldment joint.

(3) A robust estimation model of main motor power is established to determine the optimal motor energy output power prediction value to meet the global motion control requirements. The strength test of welded joints shows that the prediction results of the model can meet the engineering needs and have practical value.

REFERENCES

[1] K. K. Mugada and K. Adepu, "Influence of ridges shoulder with polygonal pins on material flow and friction stir weld characteristics of 6082 aluminum alloy," *J. Manuf. Process.*, vol. 32, pp. 625–634, Apr. 2018.

[2] K. Bruninx and E. Delarue, "A statistical description of the error on wind power forecasts for probabilistic reserve sizing," *IEEE Trans. Sustain. Energy*, vol. 5, no. 3, pp. 995–1002, Jul. 2014.

[3] S. Guo, L. Shah, R. Ranjan, S. Walbridge, and A. Gerlich, "Effect of quality control parameter variations on the fatigue performance of aluminum friction stir welded joints," *Int. J. Fatigue*, vol. 118, pp. 150–161, Jan. 2019.

[4] L. Changjun and L. Zhengjun, "Effect of post-weld heat treatment on microstructure and mechanical properties of welded joint of 7075 aluminum alloy by double-pulsed metal inert-gas welding process," *Trans. China Welding Inst.*, vol. 37, no. 10, pp. 81–84, 2016.

[5] K. H. Kim, H. S. Bang, A. F. H. Kaplan, and H. S. Bang, "Joint properties of ultra thin 430M2 ferritic stainless steel sheets by friction stir welding using pinless tool," *J. Mater. Process. Technol.*, vol. 243, pp. 381–386, May 2017.

[6] Y. Huang, X. Meng, Y. Xie, J. Li, and L. Wan, "Joining of carbon fiber reinforced thermoplastic and metal via friction stir welding with co-controlling shape and performance," *Compos. A, Appl. Sci. Manuf.*, vol. 112, pp. 328–336, Sep. 2018.

[7] Y. Huang, Z. Lv, L. Wan, J. Shen, and J. F. dos Santos, "A new method of hybrid friction stir welding assisted by friction surfacing for joining dissimilar Ti/Al alloy," *Mater. Lett.*, vol. 207, pp. 172–175, Jul. 2017.

[8] Y. Huang, Y. Xie, X. Meng, Z. Lv, and J. Cao, "Numerical design of high depth-to-width ratio friction stir welding," *J. Mater. Process. Technol.*, vol. 252, pp. 233–241, Feb. 2018.

[9] S. D. Ji, X. C. Meng, L. Ma, S. S. Gao, and R. F. Huang, "Microstructures and mechanical properties of 7N01-T4 aluminum alloy joints by active-passive filling friction stir repairing," *Mater. Sci. Eng., A*, vol. 664, pp. 94–102, May 2016.

[10] J. Shude, M. Xiangchen, S. Gao, H. Lu, L. Ma, and H. Yongxian, "Effect of rotational velocity of tool on mechanical properties of stationary shoulder friction stir welding," *Trans. China Welding Inst.*, vol. 36, no. 1, pp. 51–54, 2015.

[11] S. Hao, Y. Xinqi, and L. Dongxiao, "Microstructures and mechanical properties of 6061-T6 aluminum alloy welded by stationary shoulder friction stir welding process," *Trans. China Welding Inst.*, vol. 37, no. 8, pp. 119–123, 2016.

[12] M. Guan, Y. Wang, Y. Huang, X. Liu, X. Meng, Y. Xie, and J. Li, "Non-weld-thinning friction stir welding," *Mater. Lett.*, vol. 225, Nov. 2019, Art. no. 126506.

[13] S. Chen, H. Zhang, X. Jiang, T. Yuan, Y. Han, and X. Li, "Mechanical properties of electric assisted friction stir welded 2219 aluminum alloy," *J. Manuf. Processes*, vol. 44, pp. 197–206, Aug. 2019.

[14] X. Cheng, L. Du, G. Yang, and B. Li, "Adaptive robust control of dynamic gas pressure in a vacuum servo system," *Vacuum*, vol. 148, pp. 184–194, Feb. 2018.

[15] N. S. Tripathy, I. N. Kar, and K. Paul, "Robust dynamic event-triggered control for linear uncertain system," *IFAC-PapersOnLine*, vol. 49, no. 1, pp. 207–212, 2016.

[16] P. V. Kumar, G. M. Reddy, and K. S. Rao, "Microstructure, mechanical and corrosion behavior of high strength AA7075 aluminium alloy friction stir welds—Effect of post weld heat treatment," *Defence Technol.*, vol. 11, no. 4, pp. 362–369, Dec. 2015.

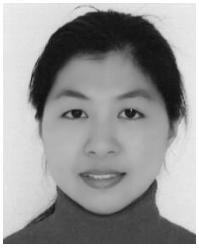

KUN ZHANG received the Ph.D. degree in material processing engineering from the Shenyang University of Technology, Shenyang, China, in 2019. Her research interests include new material welding process optimization control technology, artificial intelligence welding technology, and welding quality online predictive control technology.

ZHENGJUN LIU received the Ph.D. degree in engineering from Tianjin University, Tianjin, China, in 1995. He joined the Shenyang University of Technology, in 1987, where he is currently a Professor in material processing engineering. His research interests include development of special welding, development of metal materials, surface strengthening, and addition manufacturing.